This paper is published in IUTAM Symposium on Mesoscopic Dynamics of Fracture Process and Materials Strength, eds. H. Kitagawa and Y. Shibutani, Solid mechanics and its applications 115 (Kluwer, Dordrecht, 2004). ISBN: 1-4020-2037-6.

Chapter 1

AB INITIO STUDY OF IDEAL SHEAR STRENGTH

Shigenobu Ogata[1,2,3], Ju Li[4], Yoji Shibutani[2,3] and Sidney Yip[1]

[1]*Department of Nuclear Engineering and Department of Materials Science and Engineering, Massachusetts Institute of Technology, Cambridge, MA 02139, USA*
ogata@mech.eng.osaka-u.ac.jp, sogata@mit.edu

[2]*Department of Mechanical Engineering and Systems, Osaka University, Osaka 565-0871, Japan*

[3]*Handai Frontier Research Center, Osaka University, Osaka 565-0871, Japan*

[4]*Department of Materials Science and Engineering, Ohio State University, Columbus, OH 43210*

Abstract Ideal strength, which can be defined as the stress necessary to induce permanent deformation in a material without prior imperfections, is one of the important materials characterizations. In this study we calculate the ideal pure shear and simple shear strengths of fcc (Al, Cu, Ni, Ag) and bcc (Fe, Mo, W) metals in their common slip systems using density functional theory. We find the critical shear strains (CSS) of bcc metals ($\sim$0.18) do not depend sensitively on the material, and they are higher than fcc metals except Al. In contrast, the CSS of fcc metals spread over a wide range (0.13$\sim$0.2), with Al having extremely high CSS (0.2). As a result, although Al has smaller moduli than Cu in $\{111\}\langle 11\bar{2}\rangle$ shear, its ideal pure shear and simple shear strengths are higher than Cu. By comparative analyses of the generalized stacking fault energy and valence charge (re)distributions in Al, Ag and Cu, we conclude that the abnormally large CSS, ideal shear strength and intrinsic stacking fault energy in Al are all related to directional bonding. Cu and Ag do not have strong directional bonding. Generally, bcc metals have stronger directional bonding than the fcc metals except Al. By turning off spin polarization in our calculations, we find magnetization is a main source of bond directionality in Ni and Fe.

Keywords: Ideal shear strength, density functional theory, directional bonding, fcc metals, bcc metals, magnetization

1. Introduction

The minimum shear stress to destabilize a crystal lattice without imperfections is fundamental to our concept of materials strength and its theoretical limits under large strains [Wang95; Morris00]. With the possible exception of recent nanoindentation measurements [Gouldstone00; Li02; VanVliet03], it has not been feasible to directly measure the ideal shear strength of materials. The demonstration that this property can be reliably determined by first-principles calculations[Ogata02] therefore would have significant implications for the understanding of behavior of solids at the limit of structural stability or mechanical failure.

Here we report and substantiate our findings by probing in detail the energetics of shear deformation and valence charge redistribution during deformation for several fcc and bcc metals.

2. Method

We perform density functional theory (DFT) calculations on the following systems: fcc Ag, Cu, ferromagnetic (FM) Ni, Al and bcc W, Mo, Fe (FM), using the Vienna Ab-initio Simulation Package (VASP) [VASP]. The exchange-correlation density functional adopted is Perdew-Wang generalized gradient approximation (GGA) [Perdew92]; except for Ag, where Ceperley-Alder local density approximation (LDA) [Ceperley80; Perdew81] is used. Similarly, ultrasoft (US) pseudopotential [Vanderbilt90; VASP-US] is used, but we switch to the projector augmented-wave (PAW) method [VASP-PAW] for the difficult system of Fe. Brillouin zone (BZ) $\mathbf{k}$-point sampling is performed using the Monkhorst-Pack algorithm [Monkhorst76]. BZ integration follows the Methfessel-Paxton scheme [Methfessel89] with the smearing width chosen so the entropic free energy ("-TS" term) is less than 0.5 meV/atom. Incremental affine shear strains are imposed on each crystal along experimentally determined common slip systems to obtain the corresponding unrelaxed and relaxed energies and stresses, defined by the conditions, ϵ_{ij}=0 except $\gamma \equiv x/d_0$ (d_0 is the equilibrium separation between two adjacent atomic planes and x is the shear displacement along the Burgers vector), and σ_{ij}=0 except the resolved shear stress, respectively.

In Tables 1.1 and 1.2, the equilibrium lattice constants a_0 obtained from energy minimization are listed and compare with experimental data. The calculated relaxed and unrelaxed shear moduli G_r, G_u for the common slip systems are compared with analytical values computed based on the experimental elastic constants. The resolved shear moduli are calculated using fine meshes $\Delta\gamma = 0.5\%$-1% along the shear path, whereas coarser meshes $\Delta\gamma = 1\%$-5% are used to interpolate the resolved shear stress (σ) versus engineering shear

strain (γ) curves. Affine stress components are relaxed to within a convergence tolerance of 0.05 GPa.

3. Results and Discussions

fcc metals

At equilibrium, Ag has comparable stiffness as Al in $\{111\}\langle 11\bar{2}\rangle$ shear, and Cu is considerably stiffer, with simple and pure shear moduli greater by 65% and 25%, respectively, than Al. However, Al ends up with 70% and 32% larger ideal pure shear strength σ_m^r than Ag and Cu, respectively, because it has a longer range of strain before softening (see Fig. 1.1): γ_m=0.200 in Al, γ_m=0.145 in Ag and γ_m=0.137 in Cu. The σ_m^r/G_m^r ratio has similar trend as γ_m and the two are in fact almost linearly correlated (see Table 1.3).

Fig. 1.2 shows the iso-surfaces of valence charge density ($h \equiv V_{\rm cell}\rho_{\rm v}$, $V_{\rm cell}$ and ρ_v are the supercell volume and valence charge density, respectively). We select two h-contour values for each metal, and for Ni (FM) the difference between spin-up and down densities ($h_{\rm diff} \equiv V_{\rm cell}(\rho_{\rm v}\uparrow - \rho_{\rm v}\downarrow)$) is also shown. At the octahedral interstice in Al (Fig.1.2(a)), the pocket of charge density has cubic symmetry and is very angular in shape, with a volume comparable to the pocket centered on every ion. In contrast, Figs. 1.2(c), 1.2(d), 1.2(e), 1.2(f) show that in Cu and Ag there is no such interstitial charge pocket, the charge density being nearly spherical about each ion. Al has an inhomogeneous charge distribution in the interstitial region because of bond covalency [Feibelman90] and directional bonding [Grossman99], while Cu and Ag have relatively homogeneous charge distribution and little bond directionality. For Ni, the total charge density (spin-up plus down) shows spherical distribution (Fig.1.2(g),1.2(h)). However, the difference between spin-up and down (1.2(j)), which results in magnetization, shows a cube-shaped distribution centered on the ion, similar to that in Al (Fig.1.2(b)), even though smaller in volume. This suggests that magnetization promotes directional bonding and causes the γ_m, σ_m^r/G_m^r values of Ni to deviate from from those of Cu and Ag.

The generalized stacking fault (GSF) energy, the energy increase when two adjacent atomic planes in the crystal are sheared relative to each other, is known to play an important role in the structure and energetics of dislocations. While it is known experimentally that the intrinsic stacking fault energy is much larger in Al than in Ag and Cu, this fact has not been related to their ideal shear strengths. For this purpose, we introduce a general function (Fig. 1.3),

$$\gamma_n(x) \equiv \frac{E_n(x)}{nS_0}, \quad n = 1, 2, ... \tag{1.1}$$

where x is the relative displacement in the slip direction between two adjacent atomic planes (we focus on $\{111\}\langle 11\bar{2}\rangle$ slip here), $E_n(x)$ is the increase in to-

tal energy relative to its value at $x = 0$, with $n + 1$ being the number of planes involved in the shearing and S_0 being the cross-sectional area at $x = 0$. The series of functions $\gamma_1(x)$, $\gamma_2(x)$, ..., $\gamma_\infty(x)$, may be called the multi-plane generalized stacking fault energy, with $\gamma_1(x)$ being the conventional GSF [Zimmerman00], and $\gamma_\infty(x)$ being the affine strain energy. The intrinsic stacking fault energy $\gamma_{\rm sf}$ is $\gamma_1(b_p)$, where $\vec{b}_p$=$[11\bar{2}]a_0/6$ is the partial Burgers vector. The unstable stacking energy $\gamma_{\rm us}$, an important parameter in determining the ductility of the material [Rice94], is $\gamma_1(x_0)$, where $d\gamma_1/dx(x_0 < b_p)$=0. It is instructive to compare different $\gamma_n(x)$ of the same slip system as n varies. The difference should be relatively small from a local "glue" (shaded region in Fig. 1.3) viewpoint where we take the valence electron cloud to be the glue. We also have the asymptotic behavior at large n,

$$\gamma_n(x) \;=\; \gamma_\infty(x) + \frac{2\gamma^{\rm twin}(x)}{n} + \mathcal{O}\left(n^{-2}\right), \tag{1.2}$$

where $\gamma^{\rm twin}(b_p)$ is the unrelaxed twin boundary energy. The rate of convergence to (1.2) reflects the localization range of metallic bonding in a highly deformed bulk environment.

Unrelaxed $d\gamma_1(x)/dx$ and $d\gamma_\infty(x)/dx$ are compared in Fig. 1.4. First we note that for Ag and Cu, $d\gamma_1(x)/dx$ and $d\gamma_\infty(x)/dx$ are not very different across the entire range of shear. The fact that the sliding of a layer is effectively decoupled from that of adjacent layers indicates that bonding in Ag and Cu has nearly no bond-angle dependence. On the other hand, the same functions behave much more differently in Al, especially after $x > x_m$, at which the stress (generalized force) reaches its maximum. This is because of the coupling between two or more x's from directional bonding. Note also that $d\gamma_1(x)/dx$ of Al stays positive for an extended range, whereas $d\gamma_1(x)/dx$ of Ag and Cu "dive" into the negative sooner and deeper. Thus, while Al, Ag and Cu all have approximately the same $\gamma_{\rm us}$, when x reaches b_p and the configuration becomes an intrinsic stacking fault, Ag and Cu has recovered most of its losses in the sense of a low value of $\gamma_{\rm sf}$, whereas Al has recovered very little as its $\gamma_{\rm sf}$ remains close to $\gamma_{\rm us}$. The implication is that when a directional bond is broken, it is more difficult for the electrons to re-adapt. In contrast, non-directionally bonded systems, even if the bond angles are wrong, as long as the volumes fit as in the intrinsic stacking fault, the electrons can redistribute well and the system does not incur a large energy penalty.

To isolate the effects of magnetization, we compare the stress-displacement functions of paramagnetic Ni (Fig. 1.4(d)) with that of ferromagnetic (Fig. 1.4(c)). In paramagnetic Ni, $d\gamma_1(x)/dx$ and $d\gamma_\infty(x)/dx$ are more similar, whereas in ferromagnetic Ni relatively large differences can be seen. In other words, allowing the spin-polarization degrees of freedom promotes directional bonding in Ni.

Table 1.1. Equilibrium lattice constant (a_0), relaxed (G_r) and unrelaxed (G_u) $\{111\}\langle 11\bar{2}\rangle$ shear moduli of fcc metals.

	a_0 Å	G_r GPa	G_u GPa
Al(Calc.)	4.04	25.4	25.4
Al(Expt.)	4.03	27.4	27.6
Ni(Calc.)	3.53	60.1	79.6
Ni(Expt.)	3.51	68.8	81.0
Cu(Calc.)	3.64	31.0	40.9
Cu(Expt.)	3.62	33.3	44.4
Ag(Calc.)	4.02	25.0	32.3
Ag(Expt.)	4.07	22.4	28.7

bcc metals

Bcc metals have three common slip systems which are almost equally likely ("pencil glide") [Luo02]. We performed the same shearing tests as for fcc metals in the three slip systems. The ideal shear strain (~ 0.18) does not depend sensitively on the type of material. Moreover, the values of σ_m^r/G_m^r for the three metals are almost equal (~ 0.11) and are also close to that of Al (see Fig. 1.5, Table. 1.4). This suggests bcc metals has higher bond directionality than fcc metals except Al. Fig. 1.6 shows iso-surfaces of valence charge density. In W and Mo, we can clearly see cuboid-shaped distribution which may result in bond directionality. For Fe the total charge distribution is almost spherical. However, the difference between spin-up and down shows a cuboidal shape. So in Fe, like in Ni, magnetization is also essential for directional bonding.

Table 1.2. Equilibrium lattice constants (a_0), relaxed (G_r) and unrelaxed (G_u) shear moduli of bcc metals.

	a_0 Å	G_r GPa	G_u GPa
W $\{110\}\langle\bar{1}\bar{1}1\rangle$ (Calc.)	3.17	153.7	155.3
W $\{110\}\langle\bar{1}\bar{1}1\rangle$ (Expt.)	3.02	164.0	164.0
W $\{211\}\langle\bar{1}\bar{1}1\rangle$ (Calc.)		154.0	155.8
W $\{211\}\langle\bar{1}\bar{1}1\rangle$ (Expt.)		164.0	164.0
W $\{321\}\langle\bar{1}11\rangle$ (Calc.)		153.9	155.7
W $\{321\}\langle\bar{1}11\rangle$ (Expt.)		164.0	164.0
Mo $\{110\}\langle\bar{1}11\rangle$ (Calc.)	3.15	126.5	134.5
Mo $\{110\}\langle\bar{1}11\rangle$ (Expt.)	3.14	138.7	142.8
Mo $\{211\}\langle\bar{1}\bar{1}1\rangle$ (Calc.)		126.8	134.1
Mo $\{211\}\langle\bar{1}\bar{1}1\rangle$ (Expt.)		138.7	142.8
Mo $\{321\}\langle\bar{1}\bar{1}1\rangle$ (Calc.)		126.8	134.2
Mo $\{321\}\langle\bar{1}\bar{1}1\rangle$ (Expt.)		138.7	142.8
Fe $\{110\}\langle\bar{1}\bar{1}1\rangle$ (Calc.)	2.83	76.6	80.6
Fe $\{110\}\langle\bar{1}\bar{1}1\rangle$ (Expt.)	2.86	64.8	75.7
Fe $\{211\}\langle\bar{1}\bar{1}1\rangle$ (Calc.)		75.6	79.9
Fe $\{211\}\langle\bar{1}\bar{1}1\rangle$ (Expt.)		64.8	75.7
Fe $\{321\}\langle\bar{1}11\rangle$ (Calc.)		75.7	80.0
Fe $\{321\}\langle\bar{1}11\rangle$ (Expt.)		64.8	75.7

Table 1.3. Ideal $\{111\}\langle11\bar{2}\rangle$ shear strains and stresses of fcc metals.

	relaxed			unrelaxed		
material	γ_m^r	σ_m^r GPa	σ_m^r/G_r	γ_m^u	σ_m^u GPa	σ_m^u/G_u
Al	0.200	2.84	0.110	0.210	3.73	0.147
Ni	0.168	3.17	0.084	0.162	4.70	0.079
Cu	0.137	2.16	0.070	0.157	3.45	0.084
Ag	0.145	1.65	0.066	0.156	2.57	0.079

Table 1.4. Ideal shear strains and stresses of bcc metals.

	relaxed			unrelaxed		
material	γ_m^r	σ_m^r GPa	σ_m^r/G_r	γ_m^u	σ_m^u GPa	σ_m^u/G_u
W $\{110\}\langle\bar{1}\bar{1}1\rangle$	0.179	17.52	0.114	0.196	17.63	0.113
W $\{211\}\langle\bar{1}\bar{1}1\rangle$	0.176	17.37	0.113	0.175	17.28	0.111
W $\{321\}\langle\bar{1}11\rangle$	0.176	17.33	0.113	0.175	17.27	0.111
Mo $\{110\}\langle\bar{1}11\rangle$	0.190	15.18	0.120	0.192	16.52	0.123
Mo $\{211\}\langle\bar{1}\bar{1}1\rangle$	0.175	14.84	0.117	0.177	15.99	0.119
Mo $\{321\}\langle\bar{1}\bar{1}1\rangle$	0.176	14.87	0.117	0.175	15.93	0.119
Fe $\{110\}\langle\bar{1}\bar{1}1\rangle$	0.178	8.14	0.106	0.234	11.43	0.142
Fe $\{211\}\langle\bar{1}\bar{1}1\rangle$	0.184	7.51	0.099	0.236	9.95	0.124
Fe $\{321\}\langle\bar{1}11\rangle$	0.181	7.57	0.100	0.197	9.43	0.118

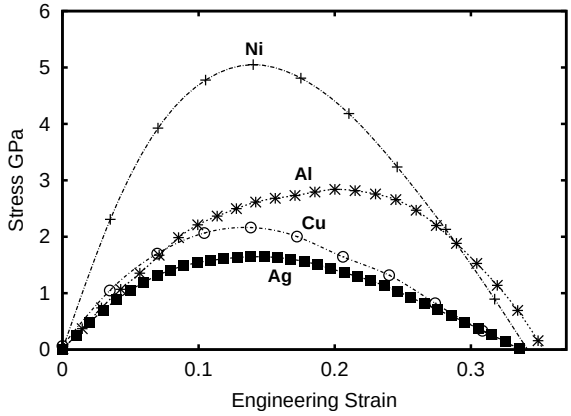

Figure 1.1. Resolved $\{111\}\langle 11\bar{2}\rangle$ shear stress vs. strain curves for fcc metals (relaxed).

Acknowledgments

SO thanks Dr. Masanori Kohyama, Prof. Hiroshi Kitagawa, Dr. Yuichiro Koizumi, and Mr. Masahiko Nishiwaki and acknowledges support by Hattori-Houkoukai fellowship. JL acknowledges support by Honda R&D Co., Ltd. and the OSU Transportation Research Endowment Program. SY acknowledges support by AFOSR, Honda R&D, DARPA/ONR, NSF-ITR, and Lawrence Livermore National Laboratory.

References

J. Wang, J. Li, S. Yip, S. Phillpot, D. Wolf, *Phys. Rev.* B **52**, 12627 (1995).
J.W. Morris and C.R. Krenn, *Phil. Mag.* A **80**, 2827 (2000).
J. Li, K.J. Van Vliet, T. Zhu, S. Yip, S. Suresh, *Nature* **418**, 307 (2002).
A. Gouldstone, H.J. Koh, K.Y. Zeng, A.E. Giannakopoulos, S. Suresh, *Acta Mat.* **48**, 2277 (2000).
K.J. Van Vliet, J. Li, T. Zhu, S. Yip, S. Suresh, *Phys. Rev.* B **67**, 104105 (2003).
S. Ogata, J. Li, S. Yip, *Science* **298** (2002) 807.
Vienna Ab-initio Simulation Package: G. Kresse and J. Hafner, *Phys. Rev.* B **47**, RC558 (1993).
G. Kresse and J. Furthmɯller, *Phys. Rev.* B **54**, 11169 (1996).
J.P. Perdew and Y. Wang, *Phys. Rev.* B **46**, 6671 (1992).
Ceperley, D. & Alder, B.J. Ground state of the electron gas by a stochastic method. *Phys. Rev. Lett.* **45**, 566-9 (1980).
Perdew, J.P. & Zunger, A. Self-interaction correction to density-functional approximations for many-electron systems. *Phys. Rev.* B **23**, 5048-79 (1981).
Vanderbilt, D. Soft self-consistent pseudopotentials in a generalized eigenvalue formalism. *Phys. Rev.* B **41**, 7892-95 (1990).
Kresse, G. & Joubert, J. From ultrasoft pseudopotentials to the projector augmented-wave method. *Phys. Rev.* B **59**, 1758-75 (1999). Blɵchl, P.E. Projector augmented-wave method. *Phys. Rev.* B **50**, 17953-79 (1994).
Monkhorst, H.J. & Pack, J.D. Special points for Brillouin-zone integrations. *Phys. Rev.* B **13**, 5188-92 (1976).
Methfessel, M. & Paxton, A.T. High-precision sampling for Brillouin-zone integration in metals. *Phys. Rev.* B **40**, 3616-21 (1989).
P.J. Feibelman, *Phys. Rev. Lett.* **65**, 729 (1990).
J.C. Grossman, A. Mizel, M. Côtɛ, M.L. Cohen, S.G. Louie, *Phys. Rev.* B **60**, 6343 (1999).
J.A. Zimmerman, H. Gao, F.F. Abraham, *Model. Simul. Mater. Sci. Eng.* **8**, 103 (2000).
J.R. Rice and G.E. Beltz, *J. Mech. Phys. Solids* **42**, 333 (1994).
W. Luo, D. Roundy, M.L. Cohen, and J.W. Morris, *Phys. Rev.* B **66**, 094110 (2002).

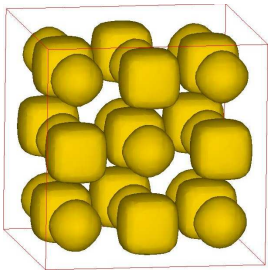

(a) Al ($h = 2.89$)

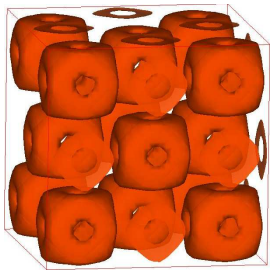

(b) Al ($h = 3.36$)

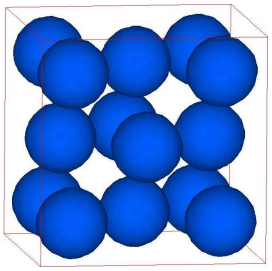

(c) Cu ($h = 9.00$)

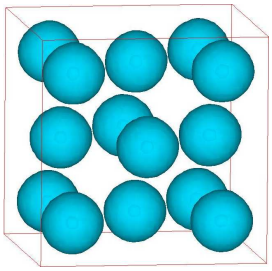

(d) Cu ($h = 20.00$)

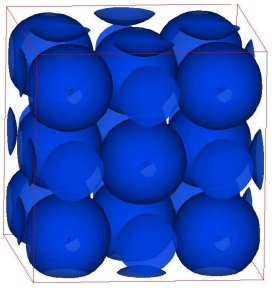

(e) Ag ($h = 5.00$)

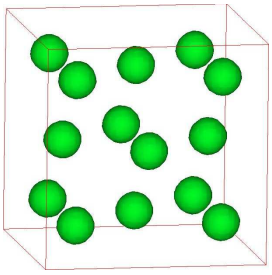

(f) Ag ($h = 10.00$)

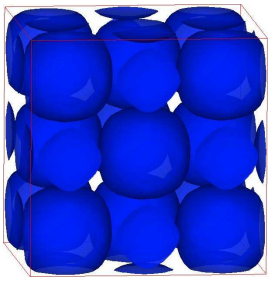

(g) Ni ($h = 3.66$)

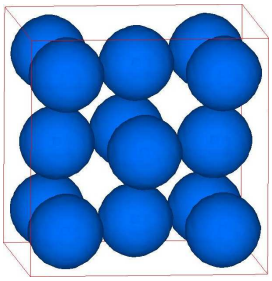

(h) Ni ($h = 8.99$)

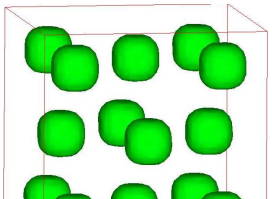

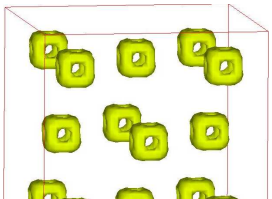

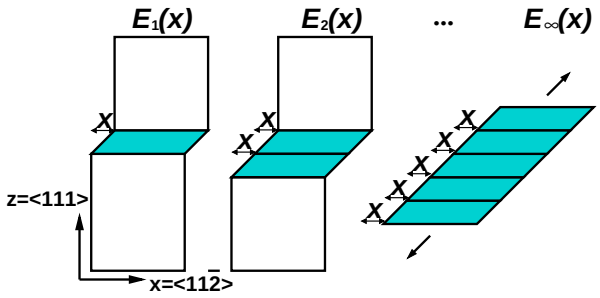

Figure 1.3. Multilayer generalized stacking fault energy

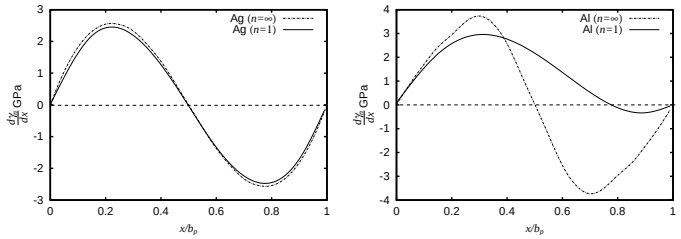

(a) Ag (b) Al

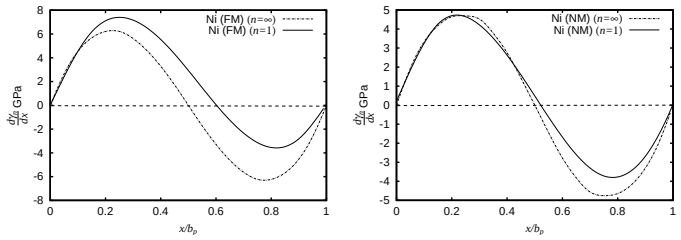

(c) Ni (FM) (d) Ni (NM)

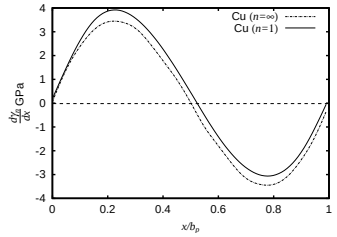

(e) Cu

Figure 1.4. Shear stress vs. displacement curves (unrelax).

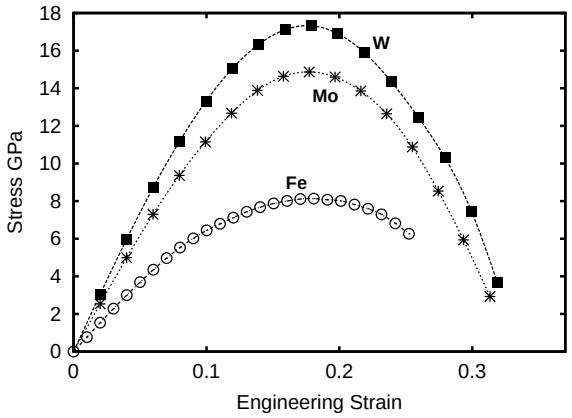

Figure 1.5. Shear stress vs. strain curves for bcc metals (relax).

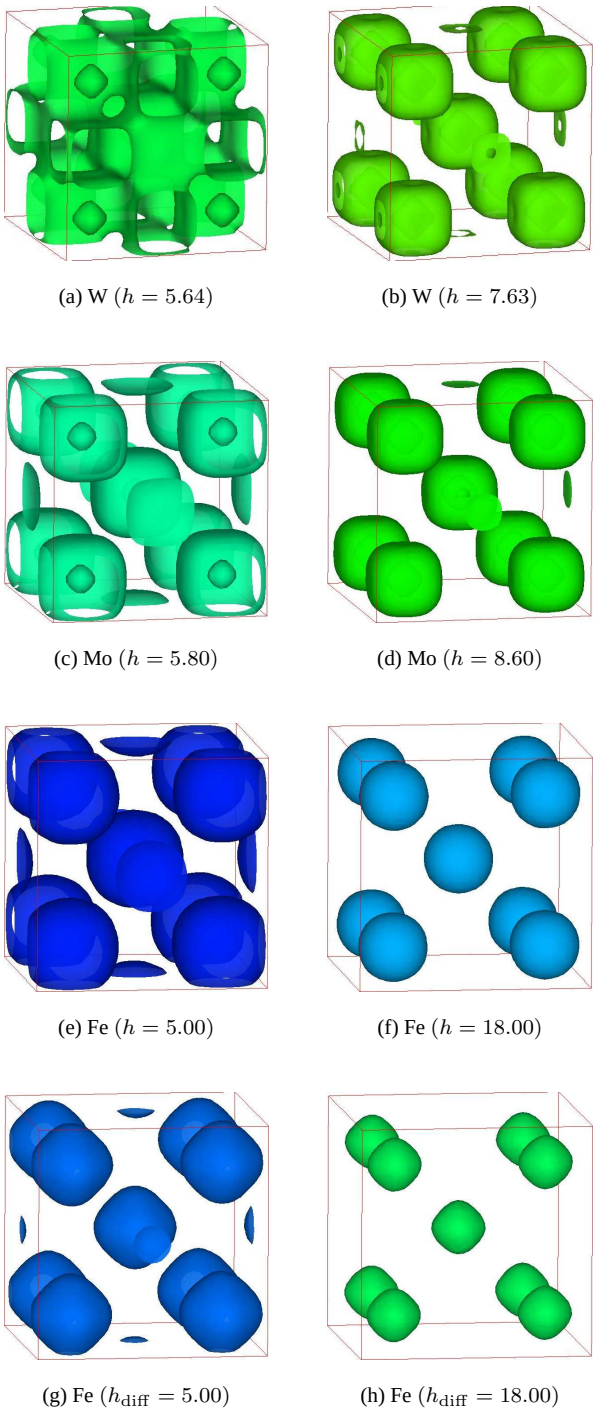

(a) W ($h = 5.64$) (b) W ($h = 7.63$)

(c) Mo ($h = 5.80$) (d) Mo ($h = 8.60$)

(e) Fe ($h = 5.00$) (f) Fe ($h = 18.00$)

(g) Fe ($h_{\mathrm{diff}} = 5.00$) (h) Fe ($h_{\mathrm{diff}} = 18.00$)

Figure 1.6. Iso-value-surface of valence charge density for bcc metals.